Published in final edited form as:
Nat Microbiol. 2016 May ; 1(5): . doi:10.1038/nmicrobiol.2016.29.

The role of the priming loop in *Influenza A virus* RNA synthesis

Aartjan J.W. te Velthuis[1,2,*], **Nicole C. Robb**[2], **Achillefs N. Kapanidis**[2], and **Ervin Fodor**[1]

[1]Sir William Dunn School of Pathology, University of Oxford, South Parks Road, OX1 3RE, Oxford, United Kingdom

[2]Clarendon Laboratory, Department of Physics, University of Oxford, Parks Road, OX1 3PU, United Kingdom

Abstract

RNA-dependent RNA polymerases (RdRps) are used by RNA viruses to replicate and transcribe their RNA genomes1. They adopt a closed, right-handed fold with conserved subdomains called palm, fingers, and thumb1,2. Conserved RdRp motifs A-F coordinate the viral RNA template, NTPs, and magnesium ions to facilitate nucleotide condensation1. For the initiation of RNA synthesis, most RdRps use either a primer-dependent or *de novo* mechanism3. The *Influenza A virus* RdRp in contrast, uses a capped RNA oligonucleotide to initiate transcription, and a combination of terminal and internal *de novo* initiation for replication4. To understand how the *Influenza A virus* RdRp coordinates these processes, we analysed the function of a thumb subdomain β-hairpin using initiation, elongation, and single-molecule FRET assays. Our data shows that this β-hairpin is essential for terminal initiation during replication, but auxiliary for internal initiation and transcription. Analysis of individual residues in the tip of the β-hairpin shows that PB1 proline 651 is critical for efficient RNA synthesis *in vitro* and in cell culture. Overall, this work advances our understanding of *Influenza A virus* RNA synthesis and identifies the initiation platform of viral replication.

Keywords

Influenza virus; RNA-dependent RNA polymerase; replication; transcription; priming loop

RNA virus RdRps catalyse the formation of the first phosphodiester bond of the nascent strand either *de novo* or in a primer-dependent manner4. A key structural feature that differentiates these two mechanisms is the priming loop, which is a loop structure that protrudes from the palm5 or thumb subdomain6,7 towards the active site of *de novo* initiating RdRps. Strictly primer-dependent RdRps lack such a structure8. An important

*Corresponding author: Sir William Dunn School of Pathology, University of Oxford, South Parks Road, Oxford OX1 3RE, United Kingdom. aartjan.tevelthuis@path.ox.ac.uk.

Author information
Correspondence and requests for materials should be addressed to AT (aartjan.tevelthuis@path.ox.ac.uk) or EF (ervin.fodor@path.ox.ac.uk).

Author contributions
AT and NR designed experiments. AT performed experiments. AT, NR, AK, and EF analysed data. AT and EF wrote manuscript.

Competing financial interest
We declare no competing financial interests.

function of the priming loop is to act as stacking platform for the initiating NTP during *de novo* initiation on the 3′ terminus of the bound single-stranded RNA (ssRNA) template6,9, *i.e.* to ensure terminal initiation. The interaction between the NTP and loop is typically mediated by a conserved aromatic residue, which buttresses the sugar-base of the initiating NTP6,9,10. A second role of the priming loop is to provide selection against dsRNA and ensure that only an ssRNA terminus is positioned into the active site10–12. This is in line with the observation that the priming loop undergoes a conformational change, either retracting like a compressed spring9 or folding into the minor groove of the product duplex5, to allow egress of a product duplex.

Some RdRps do not follow the above paradigm and use a combination of *de novo* and primer-dependent initiation to replicate and transcribe their genomes4,13. One of the best-studied examples of this type of polymerase is the RdRp of the *Influenza A virus*. The genome of this virus consists of eight negative-sense viral RNA (vRNA) segments. Each segment is bound by multiple nucleoprotein (NP) molecules and one copy of the RdRp, which yields a complex called the viral ribonucleoprotein (vRNP)4. It is in the context of this vRNP that the RdRp replicates vRNA via a complementary RNA (cRNA) intermediate and transcribes vRNA into mRNA4. All activities depend on the binding of the RdRp to conserved 5′ and 3′ terminal sequences present in each vRNA and cRNA. These terminal sequences constitute the vRNA and cRNA promoters, respectively4.

The *Influenza A virus* RdRp is formed by polymerase basic protein 1 (PB1), polymerase basic protein 2 (PB2), and polymerase acidic protein (PA) (Fig. S1a). Together these three subunits form a central core that carries out viral RNA synthesis and multiple flexible domains at the periphery of this core, including cap-binding and endonuclease domains14 (Fig. S1a). During transcription, the cap-binding and endonuclease domains enable the RdRp to snatch capped-oligonucleotides from nascent cellular RNA polymerase II (Pol II) transcripts. After alignment of a capped-oligonucleotide to the 3′ terminus of the vRNA template, the RdRp initiates transcription at position 2 or 3 of the vRNA template, depending on the sequence of the primer (Fig. 1Sb)4. In contrast, during replication the RdRp initiates *de novo* at positions 1 and 2 of the 3′ terminus of the vRNA template (terminal initiation) to copy the vRNA into a cRNA (Fig. S1c)15. When the RdRp next copies this cRNA back into vRNA, it initiates *de novo* at positions 4 and 5 of the 3′ terminus of the cRNA template (internal initiation) and produces pppApG (Fig. S1d). This dinucleotide is subsequently moved to bases 1 and 2 of the cRNA 3′ terminus, where it acts as a primer for vRNA synthesis (Fig. S1d)15.

To identify functional RdRp elements required for the initiation of *Influenza A virus* transcription and replication, we superposed the P2 initiation complex (Fig. S2) with the bat influenza A virus RdRp. The superposed structure places the tip residues of a PB1 β-hairpin (PB1 residues 642-658) close to the 3′ sugar-base of the template and the sugar-base of the initiating nucleotide (Fig. 1a). This suggests that this β-hairpin may act as a stacking platform for terminal initiation on 1U and 2C of the vRNA promoter (Fig. 1b). The β-hairpin may also act as a stacking platform for internal initiation on 4U and 5C of the cRNA promoter (Fig. 1c), but only if the 3′ terminus of the cRNA promoter can pass through the active site. A superposed structure of the bat influenza A virus RdRp with the *Poliovirus*

$3D^{pol}$ elongation complex (Fig. S3) shows that the PB1 β-hairpin does not appear to obstruct egress of the template strand and that the PB1 β-hairpin might thus support internal initiation in its modelled position. Most of the PB1 β-hairpin is unresolved in the *Influenza B* and *C virus* RdRp structures16,17, but a sequence alignment of PB1 shows that the β-hairpin is present in all influenza virus RdRps (Fig. S4).

To investigate the role of the PB1 β-hairpin in *Influenza A virus* RNA synthesis, we engineered a mutant in which the four conserved tip residues A648, H649, G650, and P651 (Fig. S4) of the influenza A/WSN/33 virus PB1 were deleted ($\Delta^{648\text{-}651}$). We first tested the activity of this mutant in cell culture by measuring the synthesis of neuraminidase (NA)-encoding viral RNA in RNP reconstitution assays (Fig. S5). As negative control for viral RNA synthesis, we used a PB1 mutant in which the two conserved aspartates of motif C were mutated to alanine ($DD^{445\text{-}446}AA$)18. Examination of the replication (vRNA and cRNA) and transcription (mRNA) products showed that $\Delta^{648\text{-}651}$ had failed to efficiently replicate and transcribe the NAvRNA (Fig. 1d). No replication or transcription was observed in the $DD^{445\text{-}446}AA$ control. Similar results were observed when we substituted the plasmid providing the NA vRNA with a plasmid expressing an NA cRNA (Fig. 1e). Together, these results suggest that the PB1 β-hairpin is critical for efficient *Influenza A virus* RNA synthesis.

The RNP reconstitution assay above did not allow us to distinguish whether transcription or replication were differentially affected due to their interdependency in cell culture. To study the role of the PB1 β-hairpin in more detail, mutant and wild-type RdRps were purified from 293T cells. All three recombinant enzymes formed hetrerotrimeric complexes with the three RdRp subunits present at an approximately 1:1:1 ratio (Fig. S6a). Moreover, wild-type and $\Delta^{648\text{-}651}$ showed similar promoter binding behaviour in a single-molecule Förster resonance energy transfer (sm-FRET) assay19 (Fig. S7), which suggests that deletion of the tip of the β-hairpin does not affect the overall conformation of the RdRp complex. We next tested their ability to support terminal and internal pppApG synthesis using [α-^{32}P]GTP and ATP on *Influenza A virus* RNA promoters. Alkaline phosphatase was added after the reaction to aid the separation of the radioactive product from the [α-^{32}P]GTP substrate and radioactive contaminants (see Fig. S8 for non-treated reactions). As shown in Fig. 1f, $\Delta^{648\text{-}651}$ exhibited a 10-fold reduced terminal initiation activity on a vRNA promoter, but internal initiation activity on a cRNA promoter remained unaffected (Fig. 1g). No pppApG synthesis was observed in the absence of RdRp or with $DD^{445\text{-}446}AA$. Using uridine to adenosine substitutions at positions 4 (4U>A) or 1 (1U>A) of the cRNA promoter we confirmed that initiation on the cRNA promoter occurred internally as expected (Fig. S9).

The finding above that absence of a full-length PB1 β-hairpin results in a 10-fold decrease in terminal, but not internal initiation, suggests that the energy requirements for these two initiation modes are different. Phosphodiester bond formation depends on multiple steps that affect the activation energy of initiation, including template and substrate binding, active site rearrangements, and the stabilisation of the initiating NTP by a priming loop. To investigate whether the 3′ UCA overhang upstream of the cRNA initiation site had an effect on the activation energy, we calculated the free energy difference ($\Delta\Delta G°$) between the template-dinucleotide duplexes that are formed during internal and terminal initiation (see Methods

and Table S1 for details) and found a $\Delta\Delta G^{\circ}$ of -1.5 kcal/mol. This difference in thermodynamic stability means that the 3′ UCA overhang upstream of the cRNA initiation site lowers the activation energy of internal *de novo* initiation 11-fold compared to terminal *de novo* initiation, which may, at least in part, explain why the RdRp does not need a full-length priming loop to stabilise the initiating ATP during internal initiation.

De novo initiation represents only the first nucleotide incorporation event in *Influenza A virus* RNA replication. To explore the role of the β-hairpin in nascent strand extension, we assayed the ability of $\Delta^{648\text{-}651}$ to synthesise pApGpC from 5′ radiolabelled pApG and CTP on a vRNA promoter. As shown in Fig. 2a, we observed no significant difference in activity between the wild-type and $\Delta^{648\text{-}651}$, while no extension of the pApG was observed in the control reactions with $DD^{445\text{-}446}AA$ or without RdRp. Similar results were observed during trinucleotide synthesis on a cRNA promoter using pApG and UTP (Fig. 2b). However, when we measured progressive elongation of an ApG in the presence of [α-^{32}P]GTP, ATP, CTP on a vRNA promoter, $\Delta^{648\text{-}651}$ exhibited significantly higher activity than the wild-type enzyme (Fig. 2c). We also measured the extension of ApG, in the presence of [α-^{32}P]GTP, ATP, and UTP on a cRNA promoter, mimicking progressive pppApG-extension after primer realignment according to the prime-realignment model (Fig. S1d). As shown in Fig. 2d, we observed that the activity of the $\Delta^{648\text{-}651}$ mutant was also higher than that of the wild-type on the cRNA promoter. This implies that a complete PB1 β-hairpin limits progressive extension during replication. When we superposed the bat influenza A virus RdRp with the *Poliovirus* $3D^{pol}$ elongation complex, the PB1 β-hairpin clashed with the product duplex (Fig. S10a). This suggests that the PB1 β-hairpin may have to undergo a conformational change to allow template-product duplex egress (Fig. S10b), which might be a rate-limiting step in *Influenza A virus* RNA synthesis.

In contrast to replication, *Influenza A virus* transcription relies on a primer-dependent initiation mechanism (Fig. S1b). To examine the role of the PB1 β-hairpin in this process, we used a radiolabelled, capped 11-nucleotide long RNA as primer that can directly anneal with the template (Fig. S1b). As shown in Fig. 3a, we observed more efficient elongation in the presence of $\Delta^{648\text{-}651}$ compared to the wild-type RdRp. A similar result was obtained when we made the transcription reaction dependent on endonuclease activity and used rabbit β-globin mRNA as cap donor in our assay (Fig. 3b). No transcription initiation was observed in the negative controls (Fig. 3a and b). Interestingly, we found an increase in the cleavage activity of $\Delta^{648\text{-}651}$ compared to the wild-type RdRp using a radiolabelled, capped 20-nucleotide long RNA in the absence of NTPs (Fig. S11). Cleavage was also observed for $DD^{445\text{-}446}AA$, but not in the buffer only control or in a reaction containing a PA endonuclease active site mutant (PA $D^{108}A$) (Fig. S11). Together, these results suggest that the full-length PB1 β-hairpin is not required for transcription initiation and that a trade-off may exist between PB1 β-hairpin-dependent terminal *de novo* initiation and primer-dependent transcription. To visualise this, we superposed the bat influenza A virus RdRp with the nascent strand of *Poliovirus* $3D^{pol}$ elongation complex and found that the PB1 β-hairpin clashes with the 3′ end of the capped-oligonucleotide if it enters the RdRp via the path of the nascent strand (see Fig. S10c). This suggests that the PB1 β-hairpin needs to undergo a conformational change to allow unobstructed capped-oligonucleotide entry and base pairing with the template. This conformational change may be similar to the change

that facilitates template-product duplex egress (Fig. S10d, line ii) or different (Fig. S10d, line iii).

To identify the amino acid at the tip of the PB1 β-hairpin that could act as stacking residue during terminal *de novo* initiation on the vRNA promoter, we examined the position of the tip residues of the PB1 β-hairpin (Fig. S4) in our structural model (Fig. 1a). P651 resides closest to the 3′ sugar-base of the template. Although not considered an aromatic residue, prolines have been found to form stacking interactions with aromatic residues20. An example can be observed in the bat influenza A virus RdRp between PB1 H363 and PA P371 (see PDB entry 4WSB). P651's position relative to the modelled position of the template and initiating NTP is, however, not compatible with stacking and more similar to the intercalating P65 of the *Escherichia coli* integration host factor (IHF)21 (Fig. S12). H649, the other residue that might stack the initiating NTP, is unresolved in the current bat influenza A virus RdRp structure and putatively oriented towards the triphosphate of the initiating NTP. Consequently, the β-hairpin will have to undergo a conformational change if one or both of these putative stacking residues is involved in supporting the initiating NTP.

To investigate the role of the amino acids at the tip of the PB1 β-hairpin, we engineered recombinant RdRps with alanine substitutions at fully conserved PB1 positions H649 ($H^{649}A$), G650 ($G^{650}A$), P651 ($P^{651}A$), and the partially conserved P647 ($P^{647}A$). All mutants were able to form a trimeric RdRp complex (Fig. S6b) and all mutants of the three conserved tip residues showed a promoter binding behaviour similar to wild-type (Fig. S7d; $P^{647}A$ was not tested), suggesting that point mutations in the tip of the β-hairpin did not affect the overall conformation of the RdRp complex. However, individual mutation of all four residues did impair terminal *de novo* initiation on a vRNA promoter with $P^{651}A$ having the strongest effect (Fig. 4a). The $DD^{445-446}AA$ control mutant showed no dinucleotide formation.

To differentiate between amino acid requirements for sugar-base and triphosphate binding, we replaced ATP with adenosine in the reactions. We found that $\Delta^{648-651}$ produced little ApG in comparison to the wild-type RdRp (Fig. S13), in agreement with the idea that the PB1 β-hairpin is important for supporting the initiating sugar-base. Next, we tested the point mutants in this assay and found that the $P^{651}A$ mutation severely reduced activity, while the other point mutations resulted in activities that were at least 50% of that of the wild-type RdRp (Fig. 4b). This suggests that P651 in the tip of the PB1 β-hairpin is the most critical for supporting the initiating sugar-base. To further investigate the role of P651, we replaced it with phenylalanine ($P^{651}F$). This mutant, which formed a trimeric complex and could bind promoter RNA (Fig. S6b and S7d), showed increased activity (~57% of wild-type) relative to $P^{651}A$ (Fig. 4a). This suggests that P651 is involved in stacking interactions, which is in line with the position of P651 close to the initiating NTP in the structural model (Fig. 1a).

H649 is an alternative amino acid in the PB1 β-hairpin that may support the initiating NTP26. Although, $H^{649}A$ showed stronger *de novo* initiation activity than $P^{651}A$ using ATP and adenosine as substrate, we investigated its potential involvement in stacking by replacing it with phenylalanine ($H^{649}F$) or arginine ($H^{649}R$, Fig. S14a). $H^{649}F$ showed decreased activity compared to $H^{649}A$, while $H^{649}R$ was as active as $H^{649}A$ (Fig. S14b).

Both mutants formed trimers and showed endonuclease activities similar to wild-type RdRp, suggesting that their overall structure is not affected by the mutations (Fig. S14a and c). These results imply that H649 is unlikely to be involved in supporting the initiating NTP through stacking.

To investigate the role of the conserved tip residues in the context of an RNP, we performed an RNP reconstitution assay in 293T cells using an NA vRNA as template (see also Fig. S5). Apart from $P^{647}A$ all point mutations greatly affected viral RNA synthesis (Fig. 4c). However, $P^{651}A$ showed the strongest reduction in cRNA synthesis compared to all the other mutants. Moreover, a phenylalanine at position 651 had a less dramatic effect on RNA synthesis than an alanine, in line with our *in vitro* experiments (Fig. 4a and b). This thus suggests that P651 is more important for the coordination of the initiating NTP than H649, but the RNP reconstitution data do demonstrate that H649 is important for the functioning of the RdRp.

In summary, the best interpretation of our results is that the PB1 β-hairpin is essential for terminal *de novo* initiation during replication (Fig. 1) and that P651 is the primary amino acid involved in the coordination of the initiating NTP during *de novo* initiation (Fig. 4). Dissection of the steps involved in viral RNA synthesis using *in vitro* assays revealed that the PB1 β-hairpin is not important for capped-oligonucleotide-dependent initiation on a vRNA template and, surprisingly, also not for internal *de novo* initiation on a cRNA template (Fig. 1). We believe that the differential requirement for a priming loop during terminal *de novo* initiation versus internal *de novo* initiation can be explained by the higher thermodynamic stability of the cRNA template-dinucleotide duplex versus the vRNA template-dinucleotide duplex, which lowers the activation energy of internal *de novo* initiation compared to terminal *de novo* initiation. However, in the absence of a ternary structure of the *Influenza A virus* RdRp with a completely resolved PB1 β-hairpin, we cannot fully exclude that P651 is an important determinant of the structural conformation of the PB1 β-hairpin and that its mutation affects terminal *de novo* replication initiation indirectly. High-resolution structural data of an influenza virus RdRp in complex with initiating NTPs and template RNA will be therefore needed to confirm our observations and shed further light on the role of the PB1 β-hairpin in the initiation of viral genome replication.

Methods

Plasmids and RNA oligonucleotides

Plasmids pcDNA-NP, pcDNA-PB1, pcDNA-PA, pcDNA-PB2-TAP, and pcDNA-PB1a have been described previously18,22,23. To construct plasmids expressing mutant PB1 proteins, the plasmid pcDNA-PB1 was subjected to site-directed mutagenesis using the primers listed in Table S2. RNA oligonucleotides used for smFRET were synthesized by IBA, and labelled, purified, and annealed as described previously19.

Sequence alignment and structural modelling

PB1 amino acid sequences from influenza A virus A/WSN/33 (H1N1) (A/WS), influenza B virus B/Michigan/22687/09 (B/MI), and influenza C virus C/JJ/50 (C/JJ) were aligned using ClustalX24 and visualised using ESPript25. To model the φ6 RNA RdRp P2 initiation complex (1HI0) into the bat influenza A virus RNA RdRp crystal structure (4WSB), we aligned active site residues 449-458 of the P2 enzyme with residues 442-449 of the bat influenza A virus RdRp PB1 subunit in Pymol 1.3. The *Poliovirus* $3D^{pol}$ elongation complex (3OL7) was aligned to the bat influenza A virus RdRp PB1 subunit using active site residues 324-332.

Purification of recombinant influenza virus RdRp

To purify influenza A/WSN/33 virus RdRp, human embryonic kidney 293T cells (stocks were originally sourced from the ATCC, stored in the Dunn School cell bank at the University of Oxford, and mycoplasma tested, but not authenticated prior to our experiments) were transfected with plasmids expressing PB1 or mutant PB1, PA, and TAP-tagged PB2 using Lipofectamine 2000 (Invitrogen) according to the manufacturer's instructions. Cells were grown in DMEM (Sigma) supplemented with 10% FCS at 37 °C and harvested 48 h post transfection. TAP-tagged RdRps were isolated through IgG sepharose chromatography (GE Healthcare) and *Tobacco etch virus* (TEV) protease cleavage as described previously23. TAP-tagged RdRps for smFRET experiments were concentrated to ~50 nM in 50 mM Hepes (pH 7.5), 10% glycerol, 500 mM NaCl, 0.05% *n*-Octyl β-D-thioglucopyranoside (OTG), and 0.5 mM tris(2-carboxyethyl)phosphine (TCEP) before storage at -80 °C in small aliquots. Wild-type and mutant RdRps were purified side-by-side and analysed through SDS-PAGE and silver staining with a SilverXpress kit (Invitrogen). All experiments were performed with at least three independently purified wild-type and mutant RdRps.

RNP reconstitution assays

This assay utilises the assembly of active vRNPs from *Influenza A virus* RdRp, NP and an NA-encoding vRNA expressed from a cellular RNA polymerase I (Pol I) promoter to measure the synthesis of viral RNA in cell culture using primer extension in the presence of a reverse transcriptase (RT) (Fig. S5). To compare the activity of mutant RdRps in cell culture, plasmids expressing the PB1, PA, PB2, NP, and the NA vRNA or cRNA of influenza A/WSN/33 virus were transfected into 293T cells using Lipofectamine 2000 (Invitrogen) according to the manufacturer's instructions. Twenty-four hours post transfection, cells were harvested, the RNA extracted using Trizol (Invitrogen), and the RNA levels assessed using reverse transcription with ^{32}P-labelled oligonucleotides against NA vRNA-derived RNA species and ribosomal 5S rRNA (Table S3). ^{32}P-derived signals were resolved on 6% denaturing PAGE, imaged using phosphorimaging on a FLA-5000 scanner (Fuji), and analysed using AIDA (RayTek) and Prism 6 (GraphPad). In all experiments, the apparent RNA levels were normalised to the 5S rRNA loading control and background corrected using the PB1 active site mutant (PB1 $DD^{445-446}AA$) signal.

sm-FRET promoter binding assays

To assess promoter binding we used a custom-built confocal microscope that allowed alternating-laser excitation (ALEX) of donor and acceptor fluorophores19,26. By placing a Cy3 donor dye on U17 of the 3′ strand and an Atto647N acceptor dye on U6 of the 5′ strand of the promoter, we minimized the possible interference of the dyes with RdRp-promoter complex formation (Fig. S7a), while keeping the expected change in distance upon promoter binding at a measurable ~10 Å (Fig. S7b). In a typical experiment, ~100 nM RdRp was pre-incubated with 1 nM double-labelled promoter RNA in buffer A (50 mM Tris-HCl (pH 8.0), 5% glycerol, 500 mM NaCl, 10 mM $MgCl_2$, 100 μg/ml BSA) for 15 min at 28 °C. Samples were diluted 10-fold in buffer A before the measurements were taken at average excitation intensities of 250 μW at 532 nm and 60 μW at 635 nm. A custom LabView code was used to detect and register signals. The output was subsequently analysed using a custom-written Matlab code as described previously19. The E^* values were plotted as one-dimensional distributions and fitted with a single Gaussian to obtain the mean E^* and the associated standard deviation.

In vitro dinucleotide synthesis assays

We performed 3-μl reactions essentially as described previously15. Briefly, for pppApG synthesis assay we incubated a reaction mixture containing 0.05 μM [α-^{32}P]GTP (3000 Ci/mmole, Perking-Elmer), 1 mM ATP, 5 mM $MgCl_2$, 1 mM DTT, 1 U/μl RNasin (Promega), 0.7 μM of promoter, 5% glycerol, 0.05% NP-40, 75 mM NaCl, 10 mM Hepes pH 7.5, and 5 ng/μl RdRp. The reactions were incubated at 30 °C for 2 h and depending on the experiment then either i) heated to 95 °C for 2 min, treated with 0.5 U shrimp alkaline phosphatase (SAP, Promega) for 30 min at 37 °C, and subsequently stopped with 3 μl stopping solution (90% formamide, 10 mM EDTA, 0.01% bromophenol blue and 0.01% xylene cyanol), or ii) directly stopped with 3 μl stopping solution. All reactions were next heated to 95 °C for 2 min and resolved by 23% denaturing PAGE. The level of [α-^{32}P]GMP incorporation was visualised using phosphorimaging as described above. To assess ApG synthesis activity, we replaced ATP in the pppApG synthesis reaction with 1 mM adenosine.

Calculation of activation energies

To calculate the fold difference in activation energy between terminal and internal *de novo* initiation, we first calculated the $\Delta\Delta G^\circ$ between the internal template-dinucleotide duplex $\begin{pmatrix} \overrightarrow{AG} \\ \underleftarrow{UCAUC} \end{pmatrix}$ and the terminal duplex $\begin{pmatrix} \overrightarrow{AG} \\ \underleftarrow{UC} \end{pmatrix}$ from melting curve analyses27,28. Since no melting data was available for 3-nucleotide 3′ overhangs, we used $\begin{pmatrix} \overrightarrow{AG} \\ \underleftarrow{CAUC} \end{pmatrix}$ to calculate the $\Delta\Delta G^\circ$ (Table S1). Using $\Delta k = e^{-\Delta\Delta G^\circ/RT}$ 29, where R is the gas constant, T is 303 °K, and $\Delta\Delta G^\circ$ is -1.5 kcal/mol, this gives a difference in activation energy of 11-fold.

In vitro pApG extension assays

Dinucleotide extension assays were performed as described above for the dinucleotide synthesis assays with the key modifications that [α-^{32}P]GTP and ATP were replaced with

radiolabelled pApG and 1 mM CTP or UTP, and that no alkaline phosphatase treatment was performed at the end of the reaction. To prepare 5′ radiolabelled pApG, we set up a 10-μl kinase reaction containing 1 mM ApG, 0.17 μM [γ-^{32}P]ATP (3000 Ci/mmole, Perking-Elmer), 1x polynucleotide kinase buffer (Invitrogen), and 1 U/μl T4 polynucleotide kinase (Invitrogen). Kinase reactions were incubated at 37 °C for 1h. The radiolabelled product was next analysed on 23% denaturing PAGE, excised, eluted overnight in deionized water, and desalted using NAP-10 columns (GE Healthcare).

In vitro ApG extension assays

To test the extension of an ApG dinucleotide, we set up 3-μl reactions containing 0.05 μM [α-^{32}P]GTP (3000 Ci/mmole, Perking-Elmer), 500 μM ApG, 1 mM ATP, 500 μM CTP or 500 μM UTP (see Fig. 4d, e), 5 μM $MgCl_2$, 1 mM DTT, 1 U/μl RNasin, 0.7 μM of promoter, 5% glycerol, 0.05% NP-40, 75 mM NaCl, 10 mM Hepes pH 7.5, and 5 ng/μl RdRp. Reactions were incubated at 30 °C for 1 h and analysed on 20% denaturing PAGE.

Capped-oligonucleotide cleavage assays

To analyse the capped-oligonucleotide cleavage activity of the RdRp, first a synthetic 20-nucleotide RNA with 5′ diphosphate (5′-ppAAUCUAUAAUAGCAUUAUCC-3′) (Chemgenes) was capped with a radiolabelled cap-1 structure in 20 μl reactions containing 1 μM RNA, 0.25 μM [α-^{32}P]GTP (3000 Ci/mmole, Perking-Elmer), 0.8 mM S-adenosylmethionine, 0.5 U/μl *Vaccinia virus* capping enzyme (NEB), and 2.5 U/μl 2′-O-methyltransferase (NEB) at 37 °C for 1h. The product was analysed on 16% denaturing PAGE, excised, eluted overnight in deionized water, and desalted using NAP-10 columns (GE Healthcare). Capped-oligonucleotide cleavage assays were performed as 4-μl reactions that contained 5 mM $MgCl_2$, 1 mM DTT, 1 U/μl RNasin, 0.7 μM of promoter, ~1500 cpm capped RNA primer, 5% glycerol, 0.05% NP-40, 75 mM NaCl, 10 mM Hepes pH 7.5, and 5 ng/μl RdRp. Reactions were incubated at 30 °C for 1 h and analysed on 20% denaturing PAGE. The background was corrected using the signal of the PA active site mutant (PA $D^{108}A$).

In vitro capped-oligonucleotide extension assays

To test the transcriptional activity of the *Influenza A virus* RdRp, we set up 3-μl reactions containing 0.05 μM [α-^{32}P]GTP (3000 Ci/mmole, Perking-Elmer), 1 mM ATP, 1 ng/μl rabbit β-globin mRNA, 500 μM CTP, 5 μM $MgCl_2$, 1 mM DTT, 1 U/μl RNasin, 0.7 μM of promoter, and 5 ng/μl RdRp. Reactions were incubated at 30 °C for 1 h. Products were analysed on 20% denaturing PAGE. To test the ability of the *Influenza A virus* RdRp to extend a capped-oligonucleotide, a synthetic 11-nucleotide RNA with 5′ diphosphate (5′-ppGAAUACUCAAG-3′) (Chemgenes) was capped as described above for the capped RNA cleavage assay. Extension assays were next performed as 4-μl reactions containing 5 mM $MgCl_2$, 1 mM DTT, 1 U/μl RNasin, 0.7 μM of promoter, 500 μM ATP, 500 μM CTP, 500 μM GTP, ~1500 cpm capped RNA primer, 5% glycerol, 0.05% NP-40, 75 mM NaCl, 10 mM Hepes pH 7.5, and 5 ng/μl RdRp. Reactions were incubated at 30 °C for 1 h and analysed on 20% denaturing PAGE.

Supplementary Material

Refer to Web version on PubMed Central for supplementary material.

Acknowledgements

This work was supported by Wellcome Trust grant 098721/Z/12/Z (to AT), Netherlands Organization for Scientific Research (NWO) grant 825.11.029 (to AT), Medical Research Council (MRC) grant MR/K000241/1 (to EF), European Commission Seventh Framework Program grant FP7/2007-2013 HEALTH-F4-2008-201418 (to AK), Biotechnology and Biological Sciences Research Council (BBSRC) grant BB/J001694/1 (to AK and EF), and a Kemp postdoctoral fellowship from Lincoln College Oxford (to AT).

References

1. te Velthuis AJ. Common and unique features of viral RNA-dependent polymerases. Cell Mol Life Sci. 2014; 71:4403–4420. [PubMed: 25080879]
2. Ng KK, Arnold JJ, Cameron CE. Structure-function relationships among RNA-dependent RNA polymerases. Curr Top Microbiol Immunol. 2008; 320:137–156. [PubMed: 18268843]
3. Kao CC, Singh P, Ecker DJ. De novo initiation of viral RNA-dependent RNA synthesis. Virology. 2001; 287:251–260. [PubMed: 11531403]
4. Fodor E. The RNA polymerase of influenza a virus: mechanisms of viral transcription and replication. Acta Virol. 2013; 57:113–122. [PubMed: 23600869]
5. Tao Y, Farsetta DL, Nibert ML, Harrison SC. RNA synthesis in a cage—structural studies of reovirus polymerase lambda3. Cell. 2002; 111:733–745. [PubMed: 12464184]
6. Butcher SJ, Grimes JM, Makeyev EV, Bamford DH, Stuart DI. A mechanism for initiating RNA-dependent RNA polymerization. Nature. 2001; 410:235–240. [PubMed: 11242087]
7. Yap TL, Xu T, Chen Y-L, Malet H, et al. Crystal structure of the dengue virus RNA-dependent RNA polymerase catalytic domain at 1.85-angstrom resolution. J Virol. 2007; 81:4753–4765. [PubMed: 17301146]
8. Thompson AA, Peersen OB. Structural basis for proteolysis-dependent activation of the poliovirus RNA-dependent RNA polymerase. EMBO J. 2004; 23:3462–3471. [PubMed: 15306852]
9. Appleby TC, Perry JK, Murakami E, Barauskas O, et al. Structural basis for RNA replication by the hepatitis C virus polymerase. Science. 2015; 347:771–775. [PubMed: 25678663]
10. Laurila MRL, Makeyev EV, Bamford DH. Bacteriophage phi 6 RNA-dependent RNA polymerase: molecular details of initiating nucleic acid synthesis without primer. J Biol Chem. 2002; 277:17117–17124. [PubMed: 11877396]
11. Hong Z, Cameron CE, Walker MP, Castro C, et al. A novel mechanism to ensure terminal initiation by hepatitis C virus NS5B polymerase. Virology. 2001; 285:6–11. [PubMed: 11414800]
12. Mosley RT, Edwards TE, Murakami E, Lam AM, et al. Structure of hepatitis C virus polymerase in complex with primer-template RNA. J Virol. 2012; 86:6503–6511. [PubMed: 22496223]
13. Morin B, Kranzusch PJ, Rahmeh AA, Whelan SPJ. The polymerase of negative-stranded RNA viruses. Curr Opin Virol. 2013; 3:103–110. [PubMed: 23602472]
14. Pflug A, Guilligay D, Reich S, Cusack S. Structure of influenza A polymerase bound to the viral RNA promoter. Nature. 2014; 516:355–360. [PubMed: 25409142]
15. Deng T, Vreede FT, Brownlee GG. Different de novo initiation strategies are used by influenza virus RNA polymerase on its cRNA and viral RNA promoters during viral RNA replication. J Virol. 2006; 80:2337–2348. [PubMed: 16474140]
16. Reich S, Guilligay D, Pflug A, Malet H. Structural insight into cap-snatching and RNA synthesis by influenza polymerase. Nature. 2014; 516:361–366. [PubMed: 25409151]
17. Hengrung N, El Omari K, Serna Martin I, Vreede FT, et al. Crystal structure of the RNA-dependent RNA polymerase from influenza C virus. Nature. 2015
18. Vreede FT, Jung TE, Brownlee GG. Model suggesting that replication of influenza virus is regulated by stabilization of replicative intermediates. J Virol. 2004; 78:9568–9572. [PubMed: 15308750]

19. Tomescu AI, Robb NC, Hengrung N, Fodor E, Kapanidis AN. Single-molecule FRET reveals a corkscrew RNA structure for the polymerase-bound influenza virus promoter. Proc Natl Acad Sci U S A. 2014
20. Luscombe NM, Laskowski RA, Thornton JM. Amino acid-base interactions: a three-dimensional analysis of protein-DNA interactions at an atomic level. Nucleic Acids Res. 2001; 29:2860–2874. [PubMed: 11433033]
21. Rice PA, Yang S, Mizuuchi K, Nash HA. Crystal structure of an IHF-DNA complex: a protein-induced DNA U-turn. Cell. 1996; 87:1295–1306. [PubMed: 8980235]
22. Fodor E, Crow M, Mingay LJ, Deng T. A single amino acid mutation in the PA subunit of the influenza virus RNA polymerase inhibits endonucleolytic cleavage of capped RNAs. J Virol. 2002; 76:8989–9001. [PubMed: 12186883]
23. Deng T, Sharps J, Fodor E, Brownlee GG. In vitro assembly of PB2 with a PB1-PA dimer supports a new model of assembly of influenza A virus polymerase subunits into a functional trimeric complex. J Virol. 2005; 79:8669–8674. [PubMed: 15956611]
24. Larkin MA, Blackshields G, Brown NP, Chenna R. Clustal W and Clustal X version 2.0. Bioinformatics. 2007; 23:2947–2948. [PubMed: 17846036]
25. Robert X, Gouet P. Deciphering key features in protein structures with the new ENDscript server. Nucleic Acids Res. 2014; 42:W320–W324. [PubMed: 24753421]
26. Santoso Y, Joyce CM, Potapova O, Le Reste L, et al. Conformational transitions in DNA polymerase I revealed by single-molecule FRET. Proc Natl Acad Sci U S A. 2010; 107:715–720. [PubMed: 20080740]
27. O'Toole AS, Miller S, Haines N, Zink MC, Serra MJ. Comprehensive thermodynamic analysis of 3 double-nucleotide overhangs neighboring Watson--Crick terminal base pairs. Nucleic acids research. 2006; 34:3338–3344. [PubMed: 16820533]
28. Sugimoto N, Kierzek R, Turner DH. Sequence dependence for the energetics of dangling ends and terminal base pairs in ribonucleic acid. Biochemistry. 1987; 26:4554–4558. [PubMed: 2444250]
29. Eyring H. The activated complex in chemical reactions. The Journal of Chemical Physics. 1935; 3:107–115.
30. Thierry E, Guilligay D, Kosinski J, Bock T. Influenza Polymerase Can Adopt an Alternative Configuration Involving a Radical Repacking of PB2 Domains. Molecular Cell. 2016; 61:1–13. [PubMed: 26748607]
31. Brownlee GG, Fodor E, Pritlove DC, Gould KG, Dalluge JJ. Solid phase synthesis of 5'-diphosphorylated oligoribonucleotides and their conversion to capped m7Gppp-oligoribonucleotides for use as primers for influenza A virus RNA polymerase in vitro. Nucleic Acids Res. 1995; 23:2641–2647. [PubMed: 7544461]

Europe PMC Funders Author Manuscripts

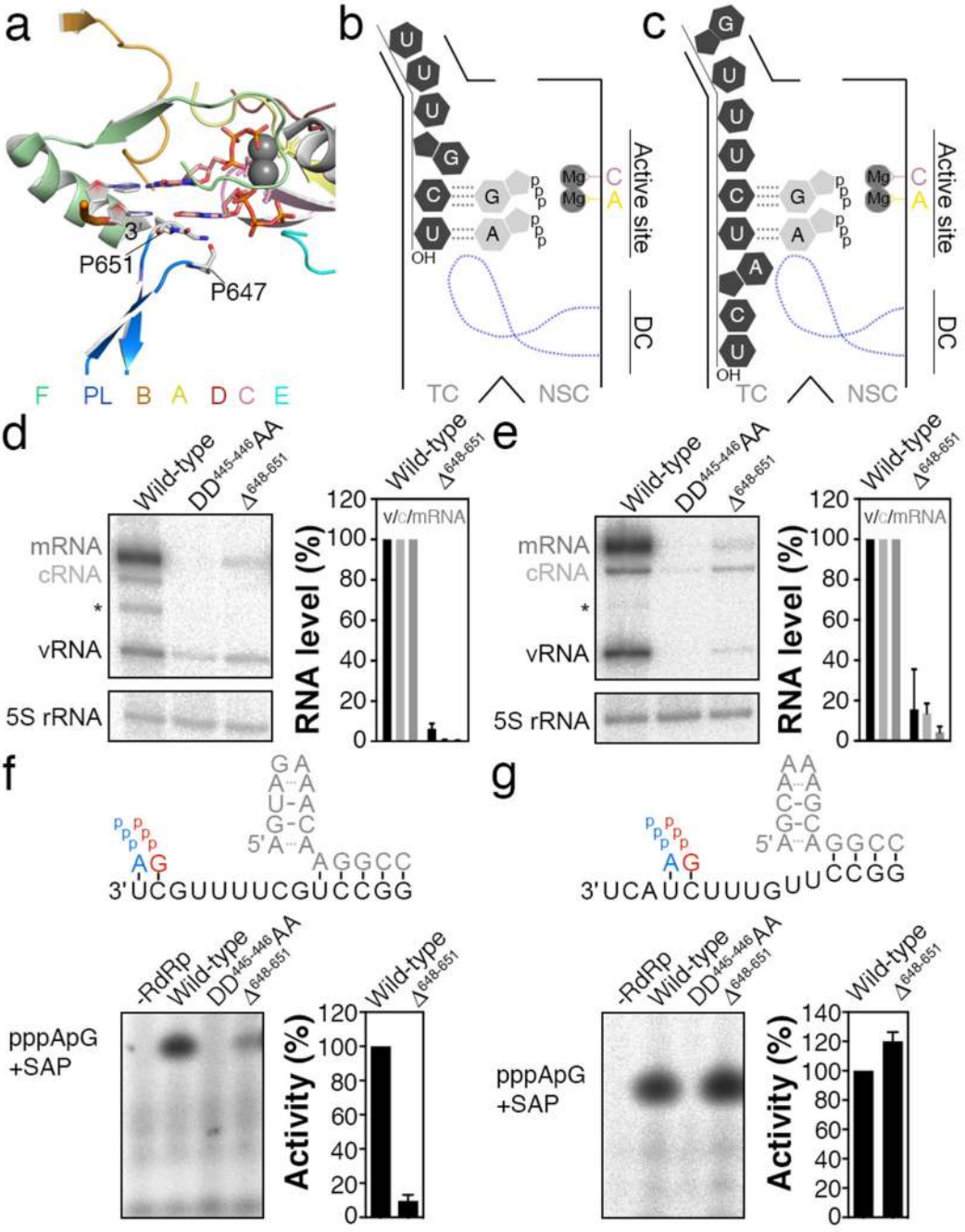

Figure 1.

The PB1 β-hairpin is essential for *Influenza A virus* RNA synthesis in cell culture and terminal *de novo* replication initiation *in vitro*. (**a**) View of the *Influenza A virus* RdRp active site with superposed ϕ6 RNA RdRp P2 initiation complex. For clarity only the conserved PB1 motifs A-F are shown, coloured yellow, orange, pink, red, cyan, and pale green, respectively. The PB1 β-hairpin (abbreviated "PL") is shown in blue. Magnesium ions that coordinate the GTPs from the ϕ6 complex are depicted as grey spheres and the 3′ end of the template strand is indicated. (**b**) Model of the *Influenza A virus* RdRp active site and

Europe PMC Funders Author Manuscripts

dsRNA channel (labelled "DC") during terminal *de novo* initiation on the 3′ end of a vRNA template (dark grey) or (**c**) during internal *de novo* initiation on the 3′ end of a cRNA template. The PB1 β-hairpin is shown as a blue dotted line. Black dotted lines indicate hydrogen bonds and grey spheres depict the magnesium ions that are coordinated by motifs A (yellow) and C (pink). The template and nascent strand exit channels are labelled "TC" and "NSC", respectively. (**d**) Analysis of the steady state RNA levels in RNP reconstitution assays (Fig. S5) with an NA vRNA and (**e**) NA cRNA template. Ribosomal 5S rRNA was used as loading control. Asterisk denotes an uncharacterised product. Graphs show the mean RNA levels with error bars indicating standard deviation ($n = 3$). (**f**) Terminal pppApG synthesis on a vRNA promoter and (**g**) internal pppApG synthesis on a cRNA promoter. The structures of the promoter strands are as in Fig. S1 and based on14,30, with the radiolabelled GTP shown in red and the unlabelled ATP in blue. The gel images show the main product after treatment with SAP to aid the separation of the radioactive product from the [α-^{32}P]GTP substrate and radioactive contaminants (see Fig. S8 for not treated reactions), and detection by autoradiography. Graphs in panels f and g show the mean percentage of polymerase activity relative to wild-type using three independent RdRp preparations. Error bars representing standard deviation ($n = 3$).

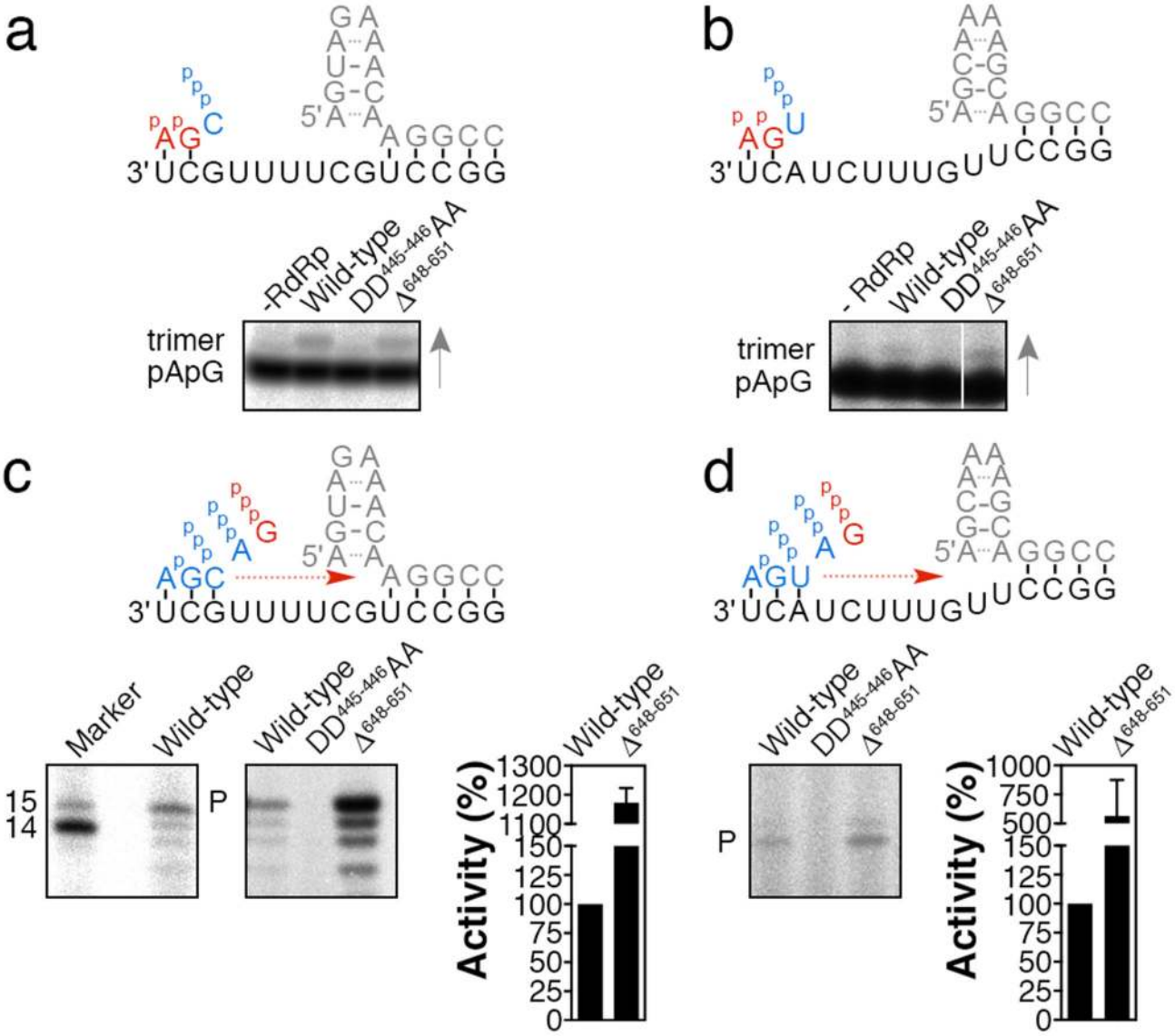

Figure 2.

The PB1 β-hairpin loop is not essential for extension during replication. (**a**) Extension of a 5′ radiolabelled pApG with CTP on a vRNA promoter and (**b**) with UTP on a cRNA promoter. Top panels show two-dimensional models of the reactions with the radiolabelled pApG shown in red and the unlabelled CTP and UTP in blue. The promoter structures are depicted as in Fig. 1. (**c**) Elongation of ApG on a vRNA promoter in the presence of ATP, CTP and [α-^{32}P]GTP, or (**d**) on a cRNA promoter in the presence of ATP, UTP and [α-^{32}P]GTP. The schematics show models of the reaction with colours as in Fig. 1. The major RNA products are labelled with "P". The graphs in Fig. 2c and d show the mean percentage of polymerase activity relative to wild-type using three independent RdRp preparations. Error bars represent standard deviation ($n = 3$).

Europe PMC Funders Author Manuscripts

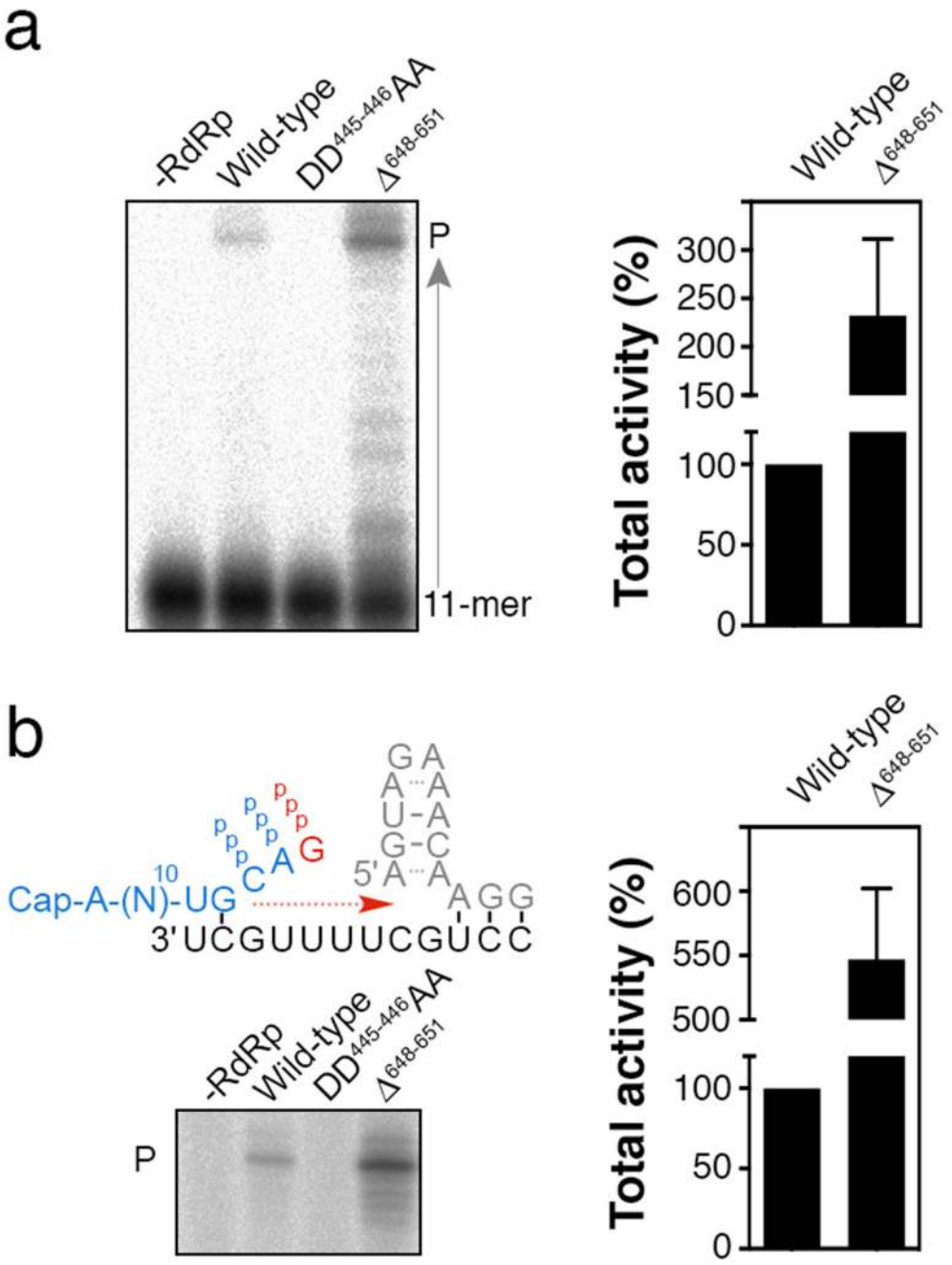

Figure 3.

The PB1 β-hairpin is not essential for transcription initiation. (**a**) Extension of a capped 11-nucleotide long RNA. Major product of the reaction is labelled with "P". (**b**) The schematic shows a two-dimensional model of a transcription reaction with β-globin mRNA as primer donor. The promoter structure and colours are as in Fig. 1. Sequence and priming site of the β-globin primer are based on31. Graphs represent average activity of three independent experiments using three independent RdRp preparations. Error bars represent standard deviation ($n = 3$).

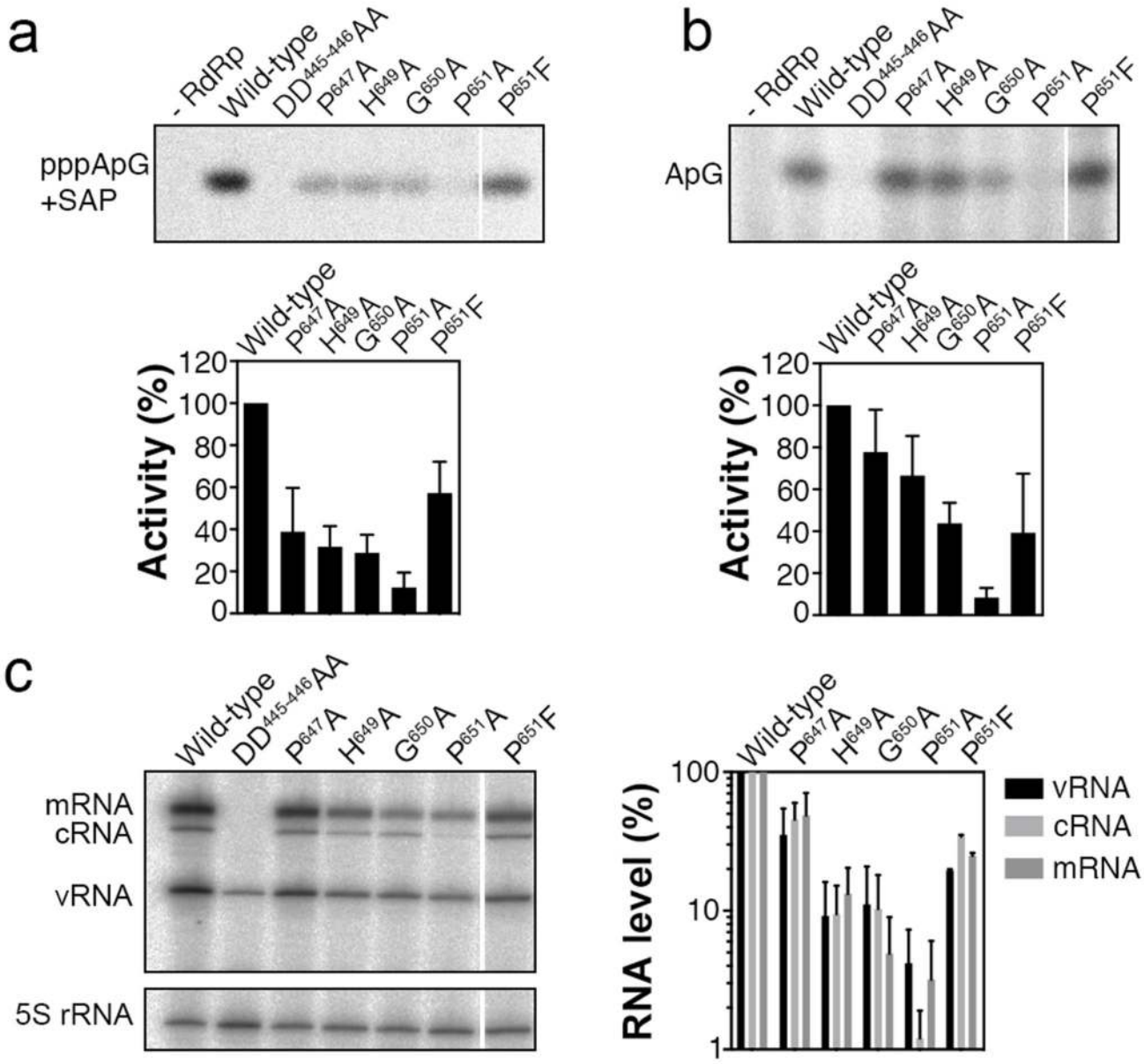

Figure 4.

PB1 P651 is essential for terminal *de novo* initiation during replication. (**a**) Synthesis of pppApG or (**b**) ApG on a vRNA promoter. The top panels show the major product (labelled "pppApG+SAP" or "ApG") after detection by autoradiography. Graphs in bottom panels show the mean polymerase activity relative to wild-type using three independent RdRp preparations. Error bars represent standard deviation ($n = 3$). (**c**) Analysis of the level of RNA synthesis on an NA vRNA template as described in Fig. S5. Ribosomal 5S rRNA was used as loading control. Graphs show the mean steady state RNA levels of three independent experiments plotted on a logarithmic scale. Error bars represent standard deviation ($n = 3$).